The mean velocity profile in three-dimensional turbulent boundary layers

By H. G. HORNUNG AND P. N. JOUBERT
Department of Mechanical Engineering, University of Melbourne

(Received 17 September 1962)

The mean velocity distribution in a low-speed three-dimensional turbulent boundary-layer flow was investigated experimentally. The experiments were performed on a large-scale model which consisted of a flat plate on which secondary flow was generated by the pressure field introduced by a circular cylinder standing on the plate. The Reynolds number based on distance from the leading edge of the plate was about 6×10^6.

It was found that the wall-wake model of Coles does not apply for flow of this kind and the model breaks down in the case of conically divergent flow with rising pressure, for example, in the results of Kehl (1943). The triangular model for the yawed turbulent boundary layer proposed by Johnston (1960) was confirmed with good correlation. However, the value of yu_τ/ν which occurs at the vertex of the triangle was found to range up to 150 whereas Johnston gives the highest value as about 16 and hence assumes that the peak lies within the viscous sublayer. Much of his analysis is based on this assumption.

The dimensionless velocity-defect profile was found to lie in a fairly narrow band when plotted against y/δ for a wide variation of other parameters including the pressure gradient. The law of the wall was found to apply in the same form as for two-dimensional flow but for a more limited range of y.

1. Introduction

The theory of turbulent boundary layers at this stage is incomplete, in that the mechanism of turbulence in boundary layers is not understood well enough to afford a direct theoretical solution of the problem throughout the entire region occupied by the boundary-layer flow. In an attempt to bridge this gap it is usual to assume the mean velocity profile in the boundary layer to follow some of various laws which in the main are based on experiment, at least at some stage of their development. Among the most successful of these laws for two-dimensional flows are the 'law of the wall' and the 'velocity defect law'.

The same procedure has been adopted in three-dimensional boundary-layer flow and the better-known assumptions about, or theoretical models for, the mean velocity profile in such flow are enumerated below.

(i) Prandtl (1946) suggested a model in which the flow in the free-stream direction is given by $u/u_1 = G(y/\delta)$ and the flow in a direction normal to both x and y by

$$w/u_1 = eG(y/\delta)\, g(y/\delta),$$

where e is the tangent of the angle between the directions of flow at the wall and in the free stream, and G and g are universal functions of y/δ with the boundary conditions

$$y = \delta\colon\ g = 0,\quad G = 1; \qquad y = 0\colon\ g = 1,\quad G = 0.$$

This model is the three-dimensional counterpart of the power-law approximation to two-dimensional boundary layers.

(ii) Moore & Richardson (1957) extended the model of von Doenhoff and Tetervin for two-dimensional layers to the case of three-dimensional flow by expressing the functions G and g above as $G\ (y/\theta_x,\ H_x)$ and $(1-y/10\theta_x)^r$, respectively.

(iii) Coles (1956) extended his own model for two-dimensional flow to the three-dimensional case and the mean-velocity profile according to this hypothesis is given by

$$\mathbf{u} = \mathbf{u}_\tau f(yu_\tau/\nu) + (\boldsymbol{\Pi}\mathbf{u}_\tau/k)\, W(y/\delta),$$

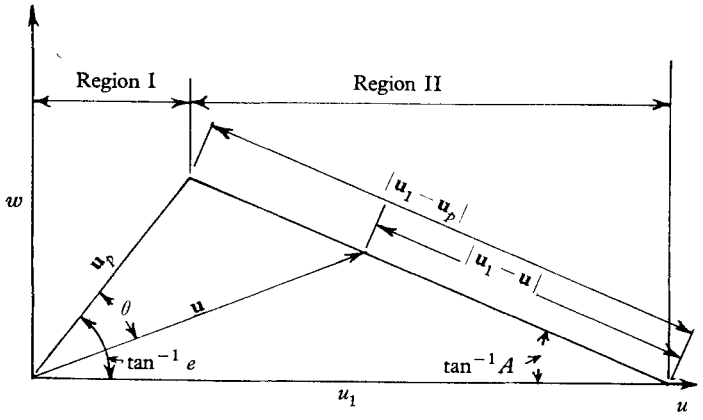

FIGURE 1. The model of Johnston.

where f is the logarithmic law of the wall, W is Coles's universal wake function, and $\boldsymbol{\Pi}$ is a tensor function of x and z. That is, the profile is made up of the vector addition of two plane profiles having the shape of the logarithmic law of the wall and of the wake function respectively.

(iv) Johnston (1960) proposed a model based on his own experimental results which specifies that in a polar plot of the mean velocity profile (velocity *vs* yaw angle), the tip of the velocity vector follows two straight lines (see figure 1). This means that $w/u_1 = eu/u_1$ in region I and $w/u_1 = A(1-u/u_1)$ in region II.

Without discussing the usefulness or further development for practical applications of these models, the experimental verification to date of the last two models will be dealt with briefly.

The Coles model has been verified by himself (1956) in the experimental results of Kuethe, McKee & Curry (1949), who used a swept wing as an experimental model, and quite good correlation existed there. The model was also confirmed, but with considerable scatter, by Blackman & Joubert (1961) who used a delta wing. Johnston verified his triangular model using the experimental results of Gruschwitz (1935), Kuethe *et al.* (1946) and Johnston (1960) with good correlation.

Because the same set of experimental results (Kuethe *et al.*) confirms both models, the question arises as to whether they are congruent. An examination of the two models reveals that they can give profiles which are to all intents and purposes the same, but only in the special case when the 'wake component' of the Coles model is much larger than the 'wall component', or, expressing this in terms of Johnston's model, when $e \gg A$. When e has about the same value as A a polar plot of the Coles model yields a curved locus of the velocity vector tip.

The Coles model is more restrictive than that of Johnston in that it specifies the distribution of mean velocity with y to some extent. The triangular model merely specifies a relation between cross-flow and main-flow components of the mean velocity profile, and no mention is made of the nature of the dependence of mean velocity on y in region II, because such a relation was not required by the analysis with which Johnston puts this model to practical use. However, it is perhaps informative to consider the implications of the straight line in region II more closely.

From the experimental fact that this line is straight in region II it can be concluded that if the profile is observed from a frame of reference moving along with the free stream, the outer profile (region II) appears to be in one plane and passes through the moving origin. In other words, the velocity defect is in a plane in region II in the same way as the velocity is in a plane in region I. This is interesting if viewed in a similar way as is sometimes done in two-dimensional layers, namely, that in the inner layer the profile obeys a 'law of the wall' dependent on effects at the wall (shear stress, viscosity) and in the outer layer it obeys a 'defect law' dependent on free-stream effects (pressure gradient, boundary-layer thickness).

The aim of this work was to produce a set of experimental results about the mean-velocity profile of low-speed three-dimensional turbulent boundary layers with secondary flow. In particular the applicability or otherwise of the two models proposed for this type of flow by Coles and Johnston was to be investigated. In order to obtain results with reasonable accuracy and some generality, the experiment was devised on a large scale, with thick boundary layers and a large field of yawed flow.

2. Experimental model

In the past, three-dimensional boundary layers have been examined mainly on swept or delta wings, with a few exceptions such as the experiments of Gruschwitz and Johnston. Since a very large wind tunnel would be needed to accommodate a swept wing on which boundary layers of about, say, 4 in. thickness can be produced, it was considered that the thickening and yawing of the boundary layer would have to occur consecutively.

This was achieved by an experimental model which consisted of a flat plate of 20 ft. length placed in the slightly divergent closed working section of the Melbourne University wind tunnel. A circular cylinder of 22 in. diameter was arranged with its axis perpendicular to the plate at about 17 ft. from the leading edge (see figure 2).

This cylinder produced a pressure field which had a strong component at right angles to the initial flow direction over a reasonably large area. The boundary layer examined was that on the flat plate about $\frac{1}{2}$ to 2 diameters upstream from the cylinder.

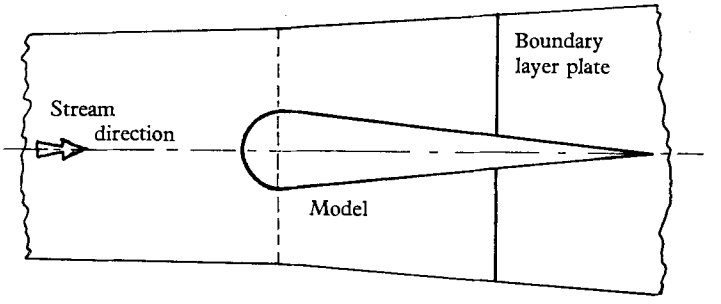

FIGURE 2. Plan view of model in wind tunnel.

3. Experimental results

By the use of a screen the turbulence level of the free stream was reduced to a value which it was hoped would be low enough to comply with the requirements for the Coles model to apply in two-dimensional flow. This requirement is that the turbulence level should be less than 0·5 %. However, the actual level in these experiments could not be reduced below 0·56 % at about 88 ft./sec, and this may have influenced the results.

The pressure field in the region upstream of the cylinder was found to be approximated by potential flow theory for a semi-infinite cylinder in an infinite uniform stream although both were very finite and the stream was decelerating slightly. The contours of experimental pressure coefficient C_{pe}, and theoretical pressure coefficient, C_{pt} (note the difference in definition below), are plotted on the same scale in figure 3 where

$$C_{pe} = \frac{p-p_B}{p_G-p_B} \quad \text{(see figure 6)} \qquad \text{and} \qquad C_{pt} = \frac{p-p_0}{\frac{1}{2}\rho V^2} = \frac{a^2}{r^2}\left(2\cos 2\phi - \frac{a^2}{r^2}\right).$$

For purposes which will be seen later we attempted to obtain, from the experimental pressure contours, the actual field in magnitude and direction, but unfortunately this was not possible with any accuracy.

A phenomenon which arises from the use of an experimental model as described above is that in the region directly in front of the cylinder the pressure rise is strong enough to cause the slow-moving particles near the wall to decelerate to negative velocities. In other words, there is a region in front of the cylinder where the flow in the inner boundary layer is away from the cylinder. On the centre-line of flow, this manifests itself in a separation point and, in the field, in a so-called 'three-dimensional separation line'. This last term is perhaps a misnomer, in that the flow does not separate along such a line and the shear stress is not zero there. Another way of looking at this phenomenon is to visualize the streamlines in the boundary layer just in front of the cylinder. For backflow to occur, the outer streamlines have to double back on themselves towards the

wall, and this results in a standing vortex wrapped around the base of the cylinder. Smoke photographs at low Reynolds number were taken to demonstrate this backflow and these are shown in figure 4, plate 1. An excellent smoke picture of the same phenomenon is also given in Thwaites (1960).

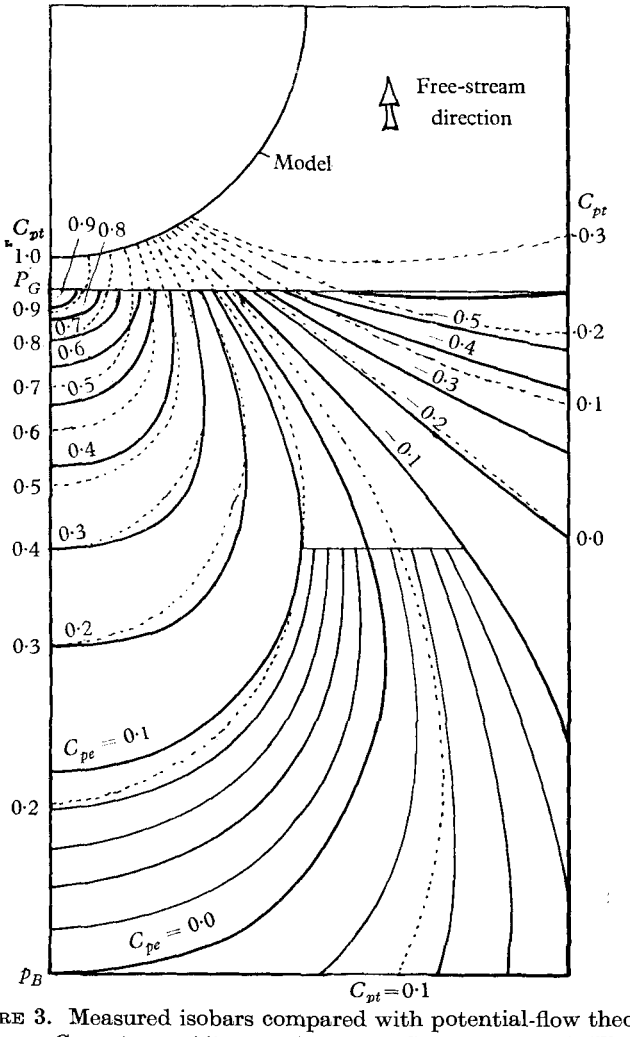

FIGURE 3. Measured isobars compared with potential-flow theory.
——, $C_{pe} = (p-p_B)/(p_G-p_B)$; – – –, $C_{pt} = (p-p_\infty)/\frac{1}{2}\rho V^2$.

4. Velocity and yaw profiles

Profiles were taken at the locations indicated in figure 5 and a typical profile is shown in figure 6.* In order to test the model proposed by Coles, the quantity $2u\sin\theta/u_1\sin\theta_1$ was plotted against y/δ. This quantity is proportional to the component of velocity normal to the shear-stress direction and so should be proportional to the Coles wake function if the model proposed by Coles is correct.

* A complete table of the observed values of u/u_1 at different values of y and θ is being held by the Editor and will be sent to readers who request it.

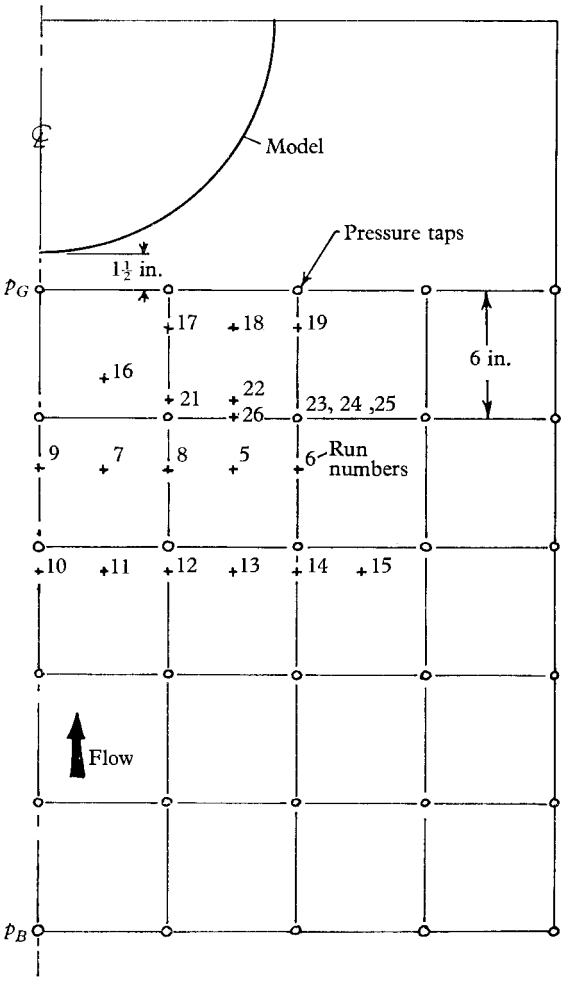

FIGURE 5. Location of stations and pressure taps.

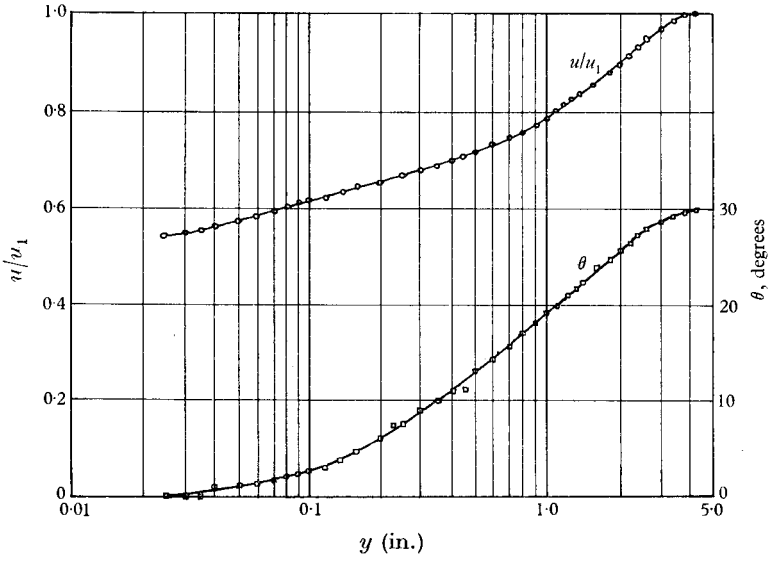

FIGURE 6. Typical velocity and yaw profile (run 24). Logarithmic plot.

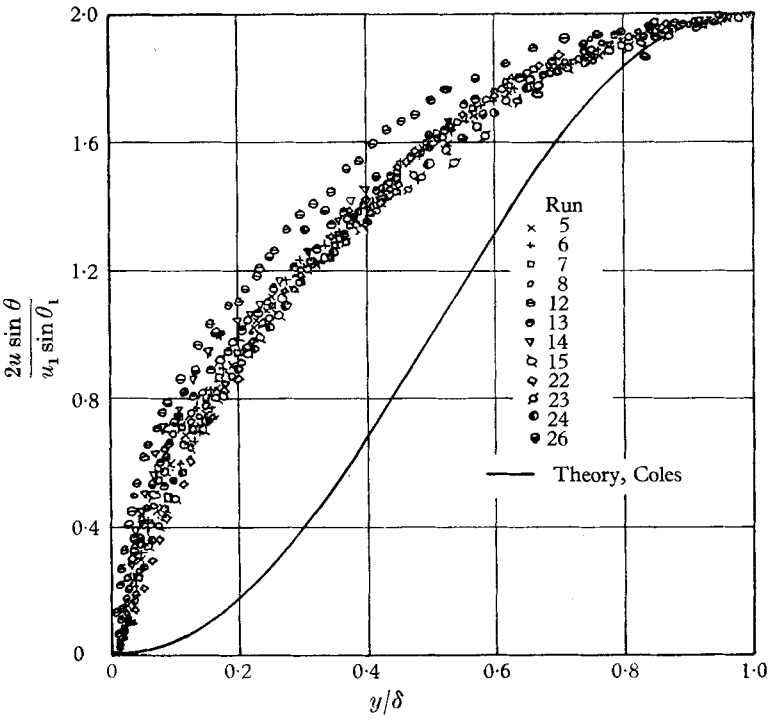

FIGURE 7. Test of the Coles wake function in yawed flow.

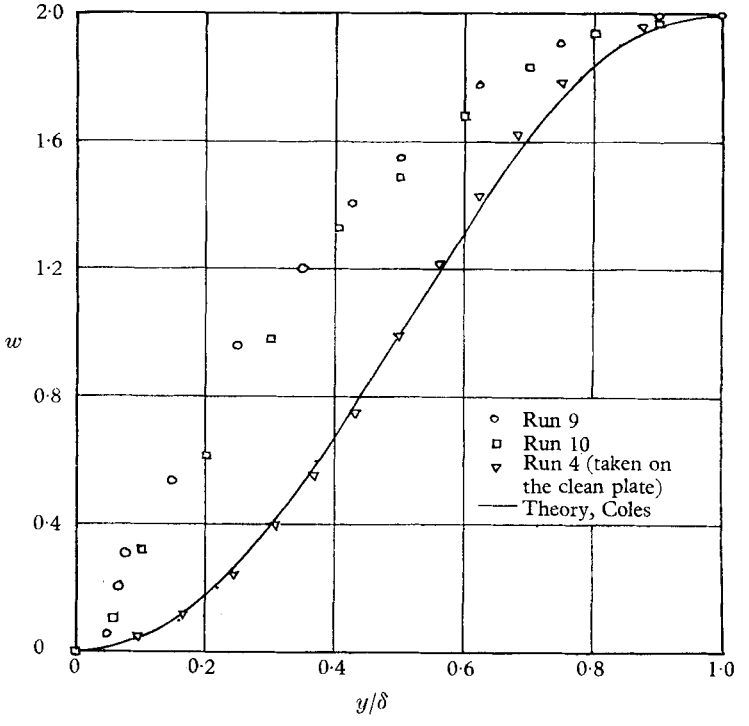

FIGURE 8. The wake component on the plane of symmetry.

A comparison of the two is given in figure 7. It can be seen that even if δ is chosen as twice the value of y for which the deviation from the logarithmic law of the wall reaches half the maximum deviation, no stretch of the imagination will make the experimental points fall on the wake-function line.

It is interesting to note that even on the centre-line of flow, where the profiles are plane in a divergent field, the Coles wake hypothesis does not hold but in the same wind tunnel and on the same plate the wake hypothesis is an accurate representation of the boundary-layer profile if the cylinder is removed (see

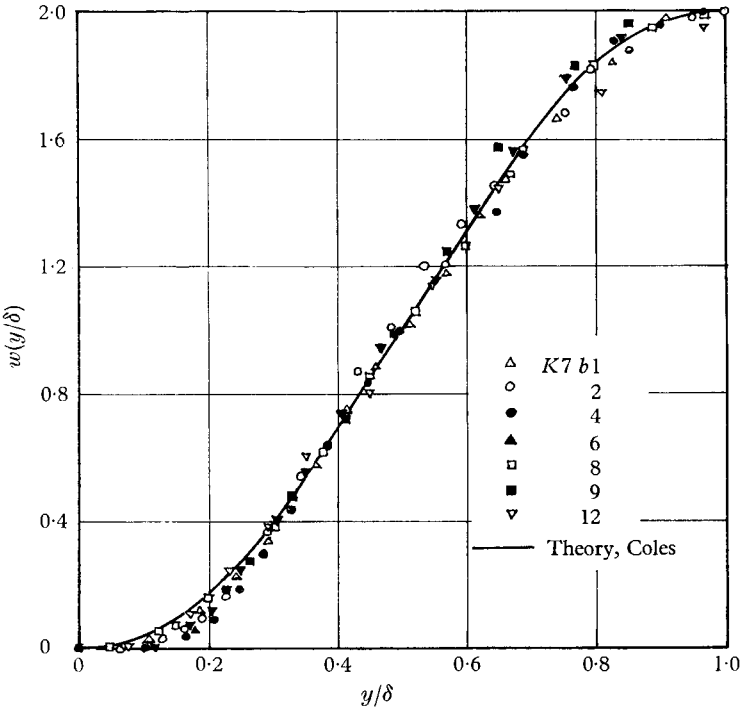

FIGURE 9. The wake function in Kehl's results taken in channel K 7b with laterally convergent flow and positive pressure gradient.

figure 8). This appears to suggest that the wake hypothesis breaks down in laterally divergent flow with rising pressure. This is confirmed by the experimental results of Kehl (1943) who performed his tests on the centre-line of one wall of divergent and convergent ducts both with positive and negative pressure gradients. These results were analysed by the authors and are shown in figures 9, 10 and 11. Notice that in the duct with divergent flow and pressure rise, the wake function becomes progressively less accurate, in a downstream direction (run K 31 is at the upstream end and run K38 at the downstream end of the duct).

The results were also plotted in the polar form u/u_1 *vs* θ in order to test the triangular model of Johnston and the result is shown in figures 12 and 13. It is seen that all the points fall quite accurately on the two straight lines and Johnston's model can be confirmed with confidence. The triangular model was found to be a reasonably accurate representation of the profile even in the region of

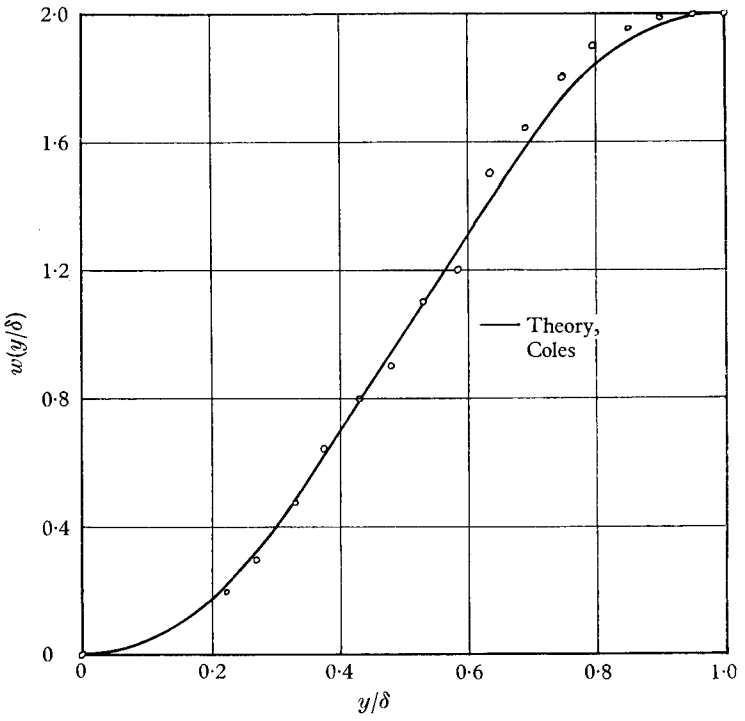

FIGURE 10. The wake function in Kehl's results taken in channel K 1 run 12 with laterally divergent flow and negative pressure gradient.

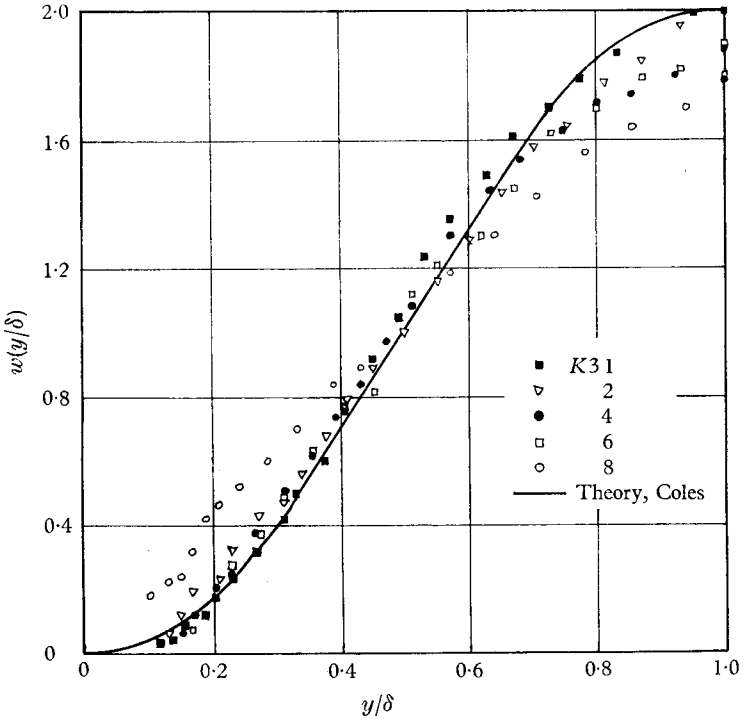

FIGURE 11. The wake function in Kehl's results taken in channel K 3 with laterally divergent flow in a positive pressure gradient.

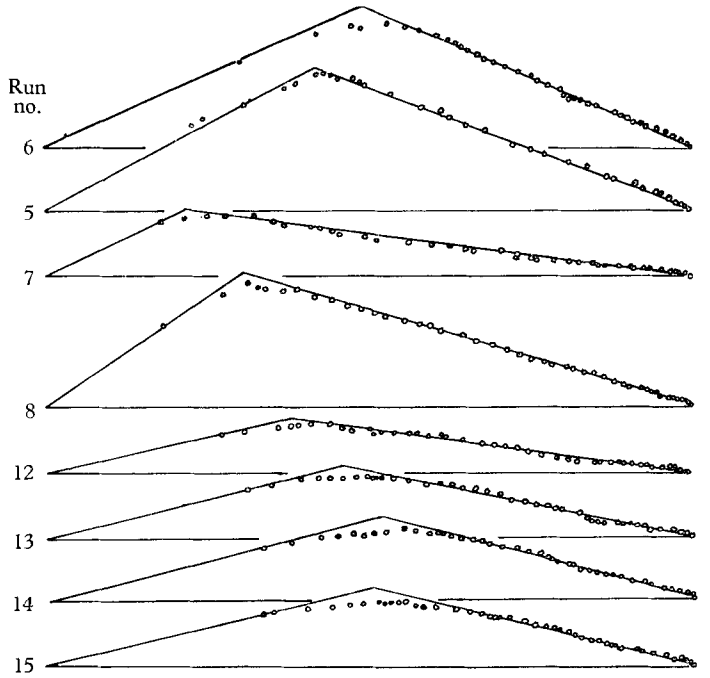

FIGURE 12. Polar plots of velocity *vs* yaw angle.

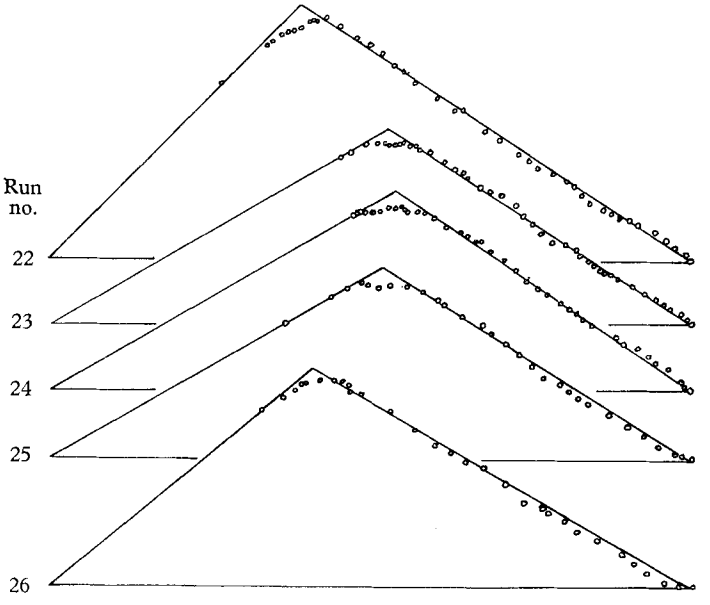

FIGURE 13. Polar plots of velocity *vs* yaw angle.

backflow, where however velocities were low in regions where the flow has a strong component normal to the wall which could not be measured, since the probe used was aligned parallel to the wall. The polar plots for the 'region of backflow' are shown in figure 14.

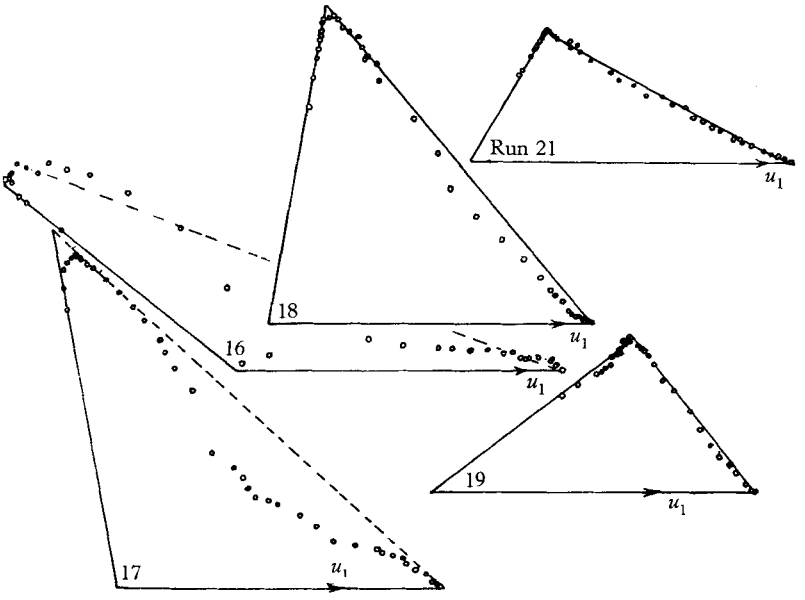

FIGURE 14. Polar plots (velocity *vs* yaw) in the region of backflow.

5. Shear stress

In order to check whether the logarithmic law of the wall still holds in three-dimensional bounday layers the wall shear stress had to be determined. This was done by using the method introduced by Clauser (1954), which assumes the law of the wall. Such a procedure appears at first sight to defeat its own purpose, but since Clauser's method relies on a fairly large portion of the velocity profile and since in these experiments at least 4 points of the profile, and sometimes 10, fell on the required slope, one can at least deduce whether a correlating quantity u_τ, say, exists or not. It is not possible to deduce that this quantity u_τ is equal to $(\tau_0/\rho)^{\frac{1}{2}}$ but it will be assumed below that it is, generalizing from two-dimensional flow.

The resulting 'law of the wall' is shown in figure 15 and the wall shear-stress field is plotted in figure 16 demonstrating the 'region of backflow'. The values of C_f' obtained by Clauser's method are given in table 1.

From the shear stress at the wall the value of yu_τ/ν at the vertex of the triangle could be determined. This was found to take values ranging from about 15 to 80 in the 'region of forward flow' and up to 150 in the 'region of backflow', thus invalidating the assumption, on which Johnston bases his analysis, that region I lies entirely within the linear sublayer.

6. The velocity defect

In order to non-dimensionalize the velocity defect, $\mathbf{u}_1 - \mathbf{u}$, it was divided by the maximum value which the defect takes in region II of the Johnston model, i.e. the dimensionless velocity defect $|\mathbf{u}_1 - \mathbf{u}|/|\mathbf{u}_1 - \mathbf{u}_p|$ was plotted *vs* y/δ in figure 18 where $\mathbf{u}_p$ is the velocity at the junction point of regions I and II.

The points from twelve runs lie within a band of scatter which is much narrower than was expected from two-dimensional boundary-layer experience, because the pressure gradient, which is one of the main quantities affecting the

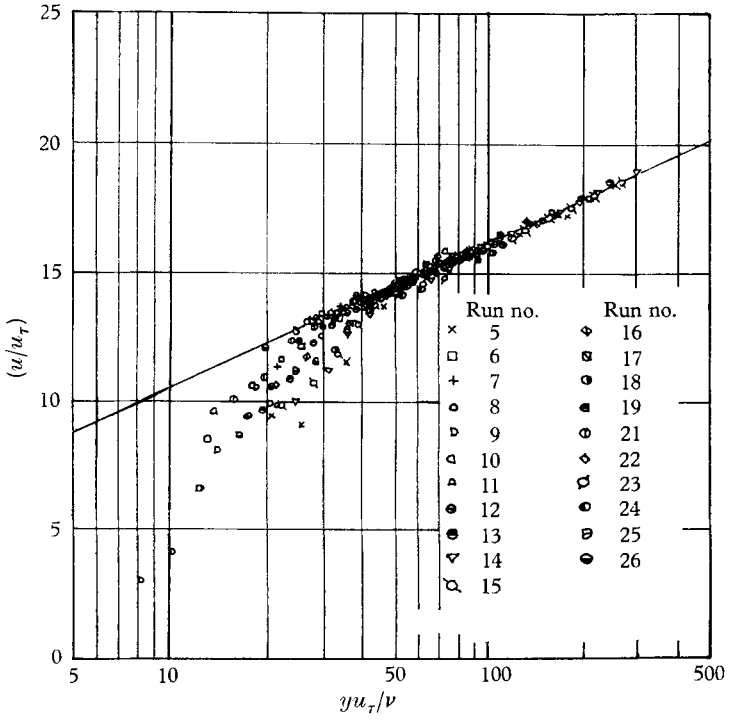

FIGURE 15. The law of the wall. ——, $u/u_\tau = 5{\cdot}6 \log_{10}(yu_\tau/\nu) + 4{\cdot}9$.

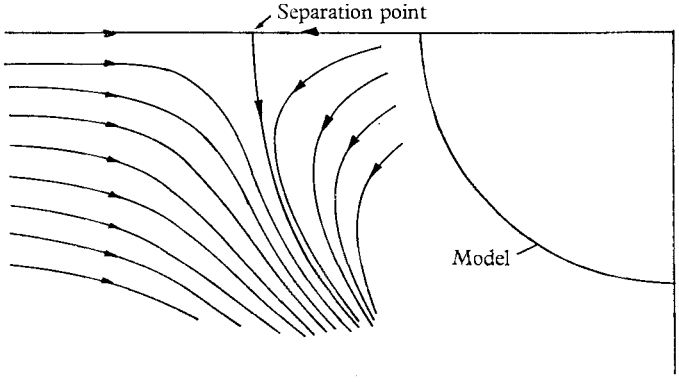

FIGURE 16. The shear-stress field (arrows in direction of flow).

shape of the defect profile of two-dimensional layers was strongly variable in the field where boundary-layer traverses were taken. It is not possible that there existed similarity between conditions at different stations, since the dimensionless parameters involved in the problem $\tau_0/(\delta^* dp/dx)$, C_f', θ_p, A, e were different in every profile. It is still possible, however, that the effects of the variation in

Run no.	u_1 (ft./sec)	θ_1 (deg.)	$C_f' \times 10^2$	α (deg.)	$\tan^{-1} A$ (deg.)	Air temp. (°C)	$\nu \times 10^4$ (ft.²/sec)
5	58·3	30·2	0·181	9·6	21·0	23–24	1·65
6	62·0	24·2	0·23	10·1	24·3	21–25	1·65
7	51·0	26·7	0·06	5·0	7·5	24–29	1·69
8	54·3	35·2	0·135	9·2	16·4	26–28	1·69
9	50·1	1·4	0·05	1·6	—	19–25	1·64
10	55·7	0·8	0·143	1·5	—	24–30	1·69
11	57·3	7·6	0·16	0·8	—	27–31	1·71
12	59·0	13·3	0·18	2·8	7·6	29–31	1·72
13	57·5	14·2	0·218	4·9	12·2	21–27	1·67
14	59·8	14·6	0·235	4·2	16·0	25–31	1·70
15	64·6	13·6	0·236	3·5	14·4	24–29	1·68
16	45·5	138·0	0·72	3·0	8·2	24–27	1·68
17	52·3	99·0	0·92	21·8	42·7	17–24	1·62
18	59·6	80·4	0·67	19·8	50·0	24–31	1·70
19	68·7	37·0	0·40	16·6	—	31–36	1·76
21	54·9	61·2	0·18	11·6	26·6	27–33	1·74
22	60·2	45·9	0·26	14·8	30·4	26–29	1·70
23	61·6	30·2	0·32	13·9	32·1	21–27	1·67
24	81·2	29·9	0·31	13·9	33·4	29–37	1·76
25	64·0	30·0	0·28	14·4	—	32–33	1·75
26	58·4	41·0	0·24	17·7	29·0	30–32	1·73

TABLE 1. Boundary conditions of the profiles

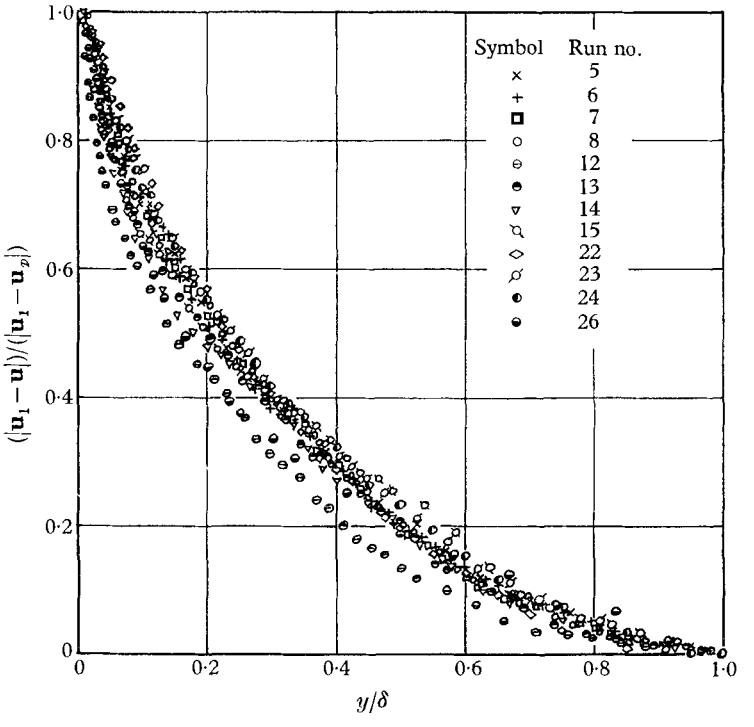

FIGURE 17. The velocity-defect profile (linear plot).

these parameters was such that they opposed each other to an extent sufficient to keep the points in figure 17 within a band of scatter such as it is. However, no dependence of the profile on any of the above parameters could be deduced because in any two runs, at least two of the five parameters were different.

It was hoped at first that an empirical relation between the four vector quantities $\mathbf{u}_1$, grad p, $\boldsymbol{\tau}_0$ and $\mathbf{u}_1 - \mathbf{u}_p$ could be deduced from the measurements taken and the velocity-defect field was plotted for that purpose. It is given in figure 18. Unfortunately, however, a number of attempts to detect a quantitative pattern in the fields remained fruitless, partly due to the fact that the magnitude of the pressure gradient could only be determined with poor accuracy from the measurements taken.

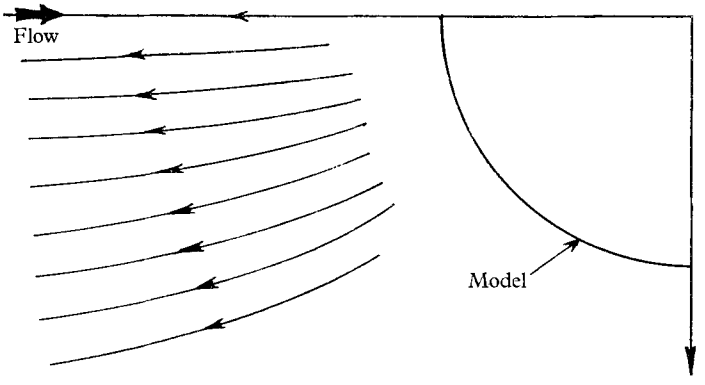

FIGURE 18. The velocity-defect field.

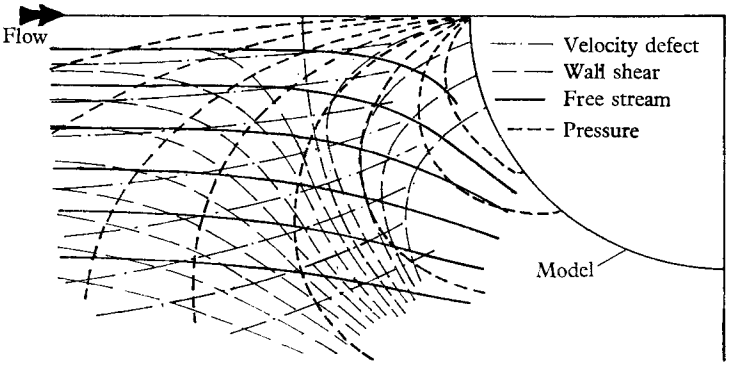

FIGURE 19. Velocity-defect, shear-stress, free-stream-velocity and pressure fields superimposed.

It is not certain, of course, that a quantitative relation between these fields can be obtained without introducing other variables, because they all represent boundary conditions only; although the velocity defect remains constant in direction through most of the layer, and grad p remains virtually constant throughout the layer (this was verified by the static pressure reading from the probe). Nevertheless, the four fields were superimposed in one diagram in figure 19 to demonstrate their qualitative interdependence.

Johnston obtained a quantitative dependence of the defect direction on the angle α through which the free-stream velocity has turned from a reference in the two-dimensional field upstream, with a number of assumptions. This relation $A = 2\alpha$, is plotted as a full line with the present experimental points in figure 20. The error in the measurement of both $\tan^{-1} A$ and α was always less than $\frac{1}{2}°$ so that the scatter of the points in figure 20 cannot be explained in terms of experimental error.

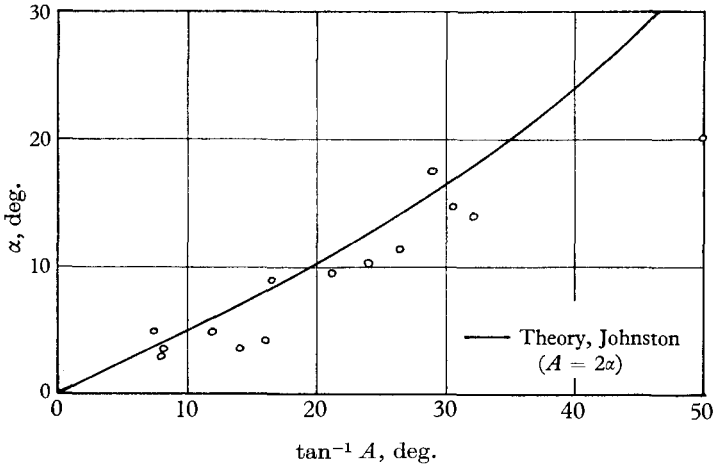

FIGURE 20. Free-stream direction and model parameter A.

7. Error evaluation

Since this article represents mainly a presentation of experimental facts, an evaluation of the errors in the recorded measurements should go with it. This is given briefly below.

Max. error in u/u_1 (at $u/u_1 = 0{\cdot}25$)	$= \pm$ 2 %
Min. error in u/u_1 (at $u/u_1 = 1{\cdot}00$)	$= \pm$ 0·5 %
Max. error in y (at $y/\delta = 0{\cdot}005$)	$= \pm$ 10 %
Min. error in y (at $y/\delta = 1{\cdot}000$)	$= \pm$ 0·05 %

(δ in all cases was approximately 4 in.)

Max. error in θ (at $\theta \doteqdot 1°$)	$= \pm$ 30 % (low speed)
Min. error in θ (at $\theta \doteqdot 1°$)	$= \pm$ 10 % (high speed)
Max. error in θ (at $\theta \doteqdot 20°$)	$= \pm$ 1·5 % (low speed)
Min. error in θ (at $\theta \doteqdot 20°$)	$= \pm$ 0·5 % (high speed)

Measurements were carried out by means of a probe consisting of one central total-head tube 1·2 mm diameter and flattened at the tip to an outside thickness of 0·025 in. (inside 0·010 in.) with yaw tubes 1·0 mm diameter on either side of it, and two static pressure tubes about $\frac{1}{4}$ in. away on each side of the three central tubes (see figure 21). The probe could be rotated and made to traverse the boundary layer by a remotely controlled mechanism. In order to check the readings taken by this probe a hot-wire anemometer was used to duplicate the results for

one profile. The effect of tunnel speed on the same profile was also looked into and the three sets of points obtained are all plotted in figure 22. It is seen that no appreciable difference exists between them, showing that the experiment was

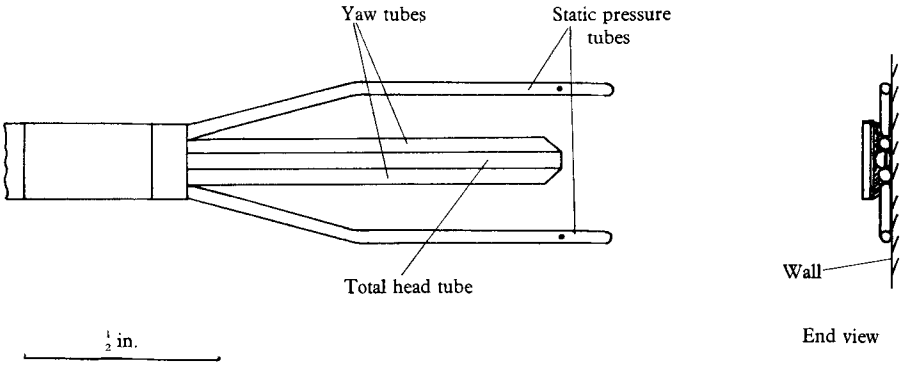

FIGURE 21. Tip of boundary-layer probe.

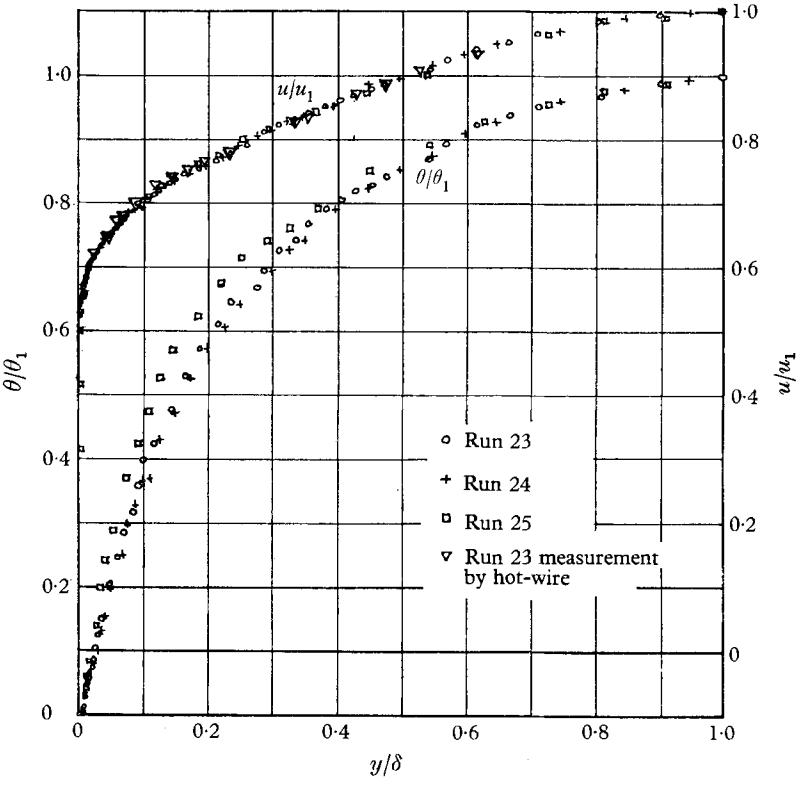

FIGURE 22. Check on probe measurements by means of hot-wire. Runs 23 and 24 at the same location, run 24 at higher speed.

carried out on a large enough scale to assume that the proximity of the wall (which has a different effect on hot-wire than it has on Pitot-tube readings) did not influence the measurements and that the flow outside the sublayer was independent of viscosity.

8. Summary of results

The model proposed by Coles for the velocity profile in three-dimensional layers does not apply to flow of the kind investigated here (namely a secondary-flow boundary layer generated by the pressure field of a circular cylinder downstream of a fully turbulent two-dimensional boundary layer) and becomes inaccurate on the centre-line of divergent flows with positive pressure gradients even in the case of the conically divergent flow of Kehl. It is possible, however, that this model applies when the flow is subjected to a transverse pressure field right from the beginning of the boundary layer as, for example, on a swept wing.

The triangular model for the polar plot of velocity *vs* yaw angle as proposed by Johnston was confirmed with good correlation; but the value of yu_τ/ν at the vertex of the triangle was found to range up to 150 whereas Johnston gives the highest value as about 16. This contradicts the assumption made by Johnston that region I lies within the viscous sublayer. This assumption is the basis of much of Johnston's analysis. The approximate relation $A = 2\alpha$ given by Johnston was found to be approximately true only for small values of A. Since the scatter of points on the plot of $\tan^{-1} A$ *vs* α is much worse than can be explained in terms of experimental error, it is thought that a third parameter enters the relation $A(\alpha)$.

The law of the wall applies to three-dimensional boundary layers in the same form as it does to two-dimensional layers up to the point where the boundary layer becomes yawed.

The velocity defect is in a plane for the outer 97–99 % of the boundary layer. This, of course, was implied by Johnston in proposing the triangular model, but it is thought here that this is a most significant phenomenon which simplifies the problem of the yawed boundary layer and so is well worth stating explicitly. The velocity defect, if non-dimensionalized by dividing it by the velocity defect at the vertex of the triangular model and if plotted versus y/δ, falls within a reasonably narrow band even for widely varying values of pressure gradient, shear stress, velocity-defect direction and free-stream velocity. However, no dependence on any of these variables could be deduced because in any two runs, at least two of the four parameters were different. The defect profile is similar in form to the defect profile obtained in two-dimensional layers

REFERENCES

Blackman, D. R. & Joubert, P. N. 1960 *J. Roy. Aero. Soc.* **64**, 692.

Clauser, F. 1954 *J. Aero. Sci.* **21**, 91.

Coles, D. 1956 *J. Fluid Mech.* **1**, 191.

Gruschwitz, E. 1935 *Ing. Archiv.* **6**, 355.

Johnston, J. 1960 *Trans. A.S.M.E.* Series D, **82**, 233.

Kehl, A. 1943 *Ing. Archiv.* **13**, 293.

Kuethe, A., McKee, P. & Curry, W. 1949 *N.A.C.A. T.N.* no. 1946.

Moore, R. W. & Richardson, D. L. 1957 *Trans. A.S.M.E.* **79**, 1789.

Prandtl, L. 1946 *M.A.P. Volkenrode* (Rep. & Trans. no. 64).

Thwaites, B. 1960 *Incompressible Aerodynamics*, p. 552. Oxford: Clarendon Press.

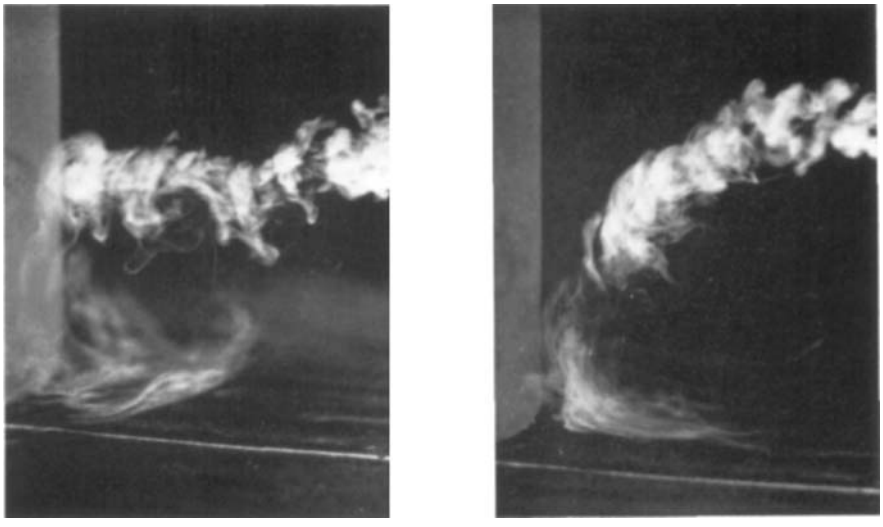

FIGURE 4, plate 1. Smoke photographs. Cigarette smoke was introduced into the flow by means of a thin tube at about 3 in. from the plate, i.e. inside the boundary layer, as can be seen from the turbulent nature of the flow. Air speed was approximately 15 ft./sec, $Re_x \approx 1{\cdot}5 \times 10^6$. The white line in the foreground is the flow centre-line. Notice the path of the smoke directly in front of the model.